ACS OMEGA

http://pubs.acs.org/journal/acsodf

Mini-Review

Recent Advances in the Carrier Mobility of Two-Dimensional Materials: A Theoretical Perspective

Showkat Hassan Mir, Vivek Kumar Yadav, and Jayant Kumar Singh*

Cite This: *ACS Omega* 2020, 5, 14203−14211

Read Online

ACCESS | Metrics & More | Article Recommendations

ABSTRACT: Since the breakthrough of graphene, 2D materials have engrossed tremendous research attention due to their extraordinary properties and potential applications in electronic and optoelectronic devices. The high carrier mobility in the semiconducting material is critical to guarantee a high switching speed and low power dissipation in the corresponding device. Here, we review significant recent advances and important new developments in the carrier mobility of 2D materials based on theoretical investigations. We focus on some of the most widely studied 2D materials, their development, and future applications. Based on the current progress in this field, we conclude the review by providing challenges and an outlook in this field.

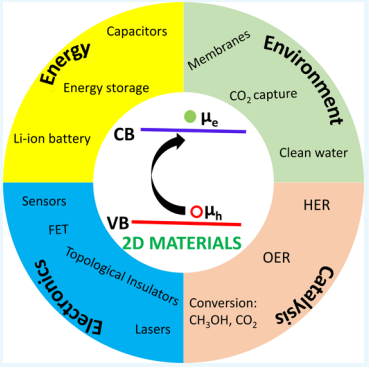

INTRODUCTION

For the past two decades, two-dimensional (2D) materials have been widely investigated due to their exceptional properties. The rise of 2D materials started with the discovery of graphene: a single atomic layer of graphite with sp^2 hybridization.[1] Since the discovery of graphene in 2004, 2D materials have shown tremendous research progress in graphene and graphene-like nanomaterials such as phosphorene, silicene, antimonene, graphitic carbon, and hexagonal boron nitride (h-BN) (g-C_3N_4). Therefore, the resulting library of 2D materials is vast and shows a wide spectrum of properties ranging from the insulators to the best conductors and from the softest to the strongest. The summarized data of 2D material families as a chart are presented in Figure 1. All the 2D materials exhibit a sheet-like structure with a thickness that is one or a few atomic layers. In contrast, the lateral dimensions can be in micrometer scale or even larger in size. Because of the inherent atomic thickness and sheet-like structure, the electronic, optoelectronic, physical, and chemical properties of 2D materials are profoundly attractive and have generated enormous research interest. Due to their atomic thickness, the transport of carriers (electron/hole), phonons, and photons is strongly confined to the plane, which then leads to unusual changes in the electronic, thermal, and optical properties.[2−6]

For instance, graphene is recognized to have anomalous properties such as ultrahigh carrier mobility, large Young's modulus, high specific surface area, exceptional optical transparency, and excellent electric and thermal conductivity. Nevertheless, it is important to remember that despite similar

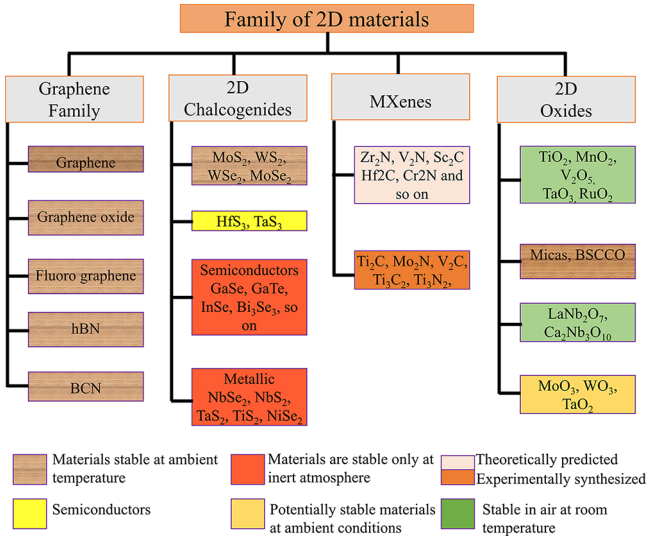

Figure 1. Chart showing library of 2D materials.[5,6,10] BSCCO is bismuth strontium calcium copper oxide, and BCN or borocarbonitride is a composite of boron, carbon, and nitrogen.

Received: April 13, 2020
Accepted: May 29, 2020
Published: June 11, 2020

https://dx.doi.org/10.1021/acsomega.0c01676
ACS Omega 2020, 5, 14203−14211

structural characteristics the properties of different members in the 2D families can be distinct owing to the different composition of each member. For example, contrary to the graphene, which is chemically inert and has no intrinsic band gap, transition metal dichalcogenides (TMDCs) show versatile chemistry, and many of them exhibit finite band gaps. Monolayer black phosphorus (phosphorene) also exhibits a sizable band gap and high carrier mobility. The outstanding properties of 2D materials make them highly interesting in fundamental studies as well as in a broad spectrum of technological applications such as electronics, optoelectronics, catalysis, CO_2 capture, energy storage/conversion, and the sensor.[7−9]

Figure 2 shows the crystal structures of some of the 2D materials. The high carrier mobility is one of the primary

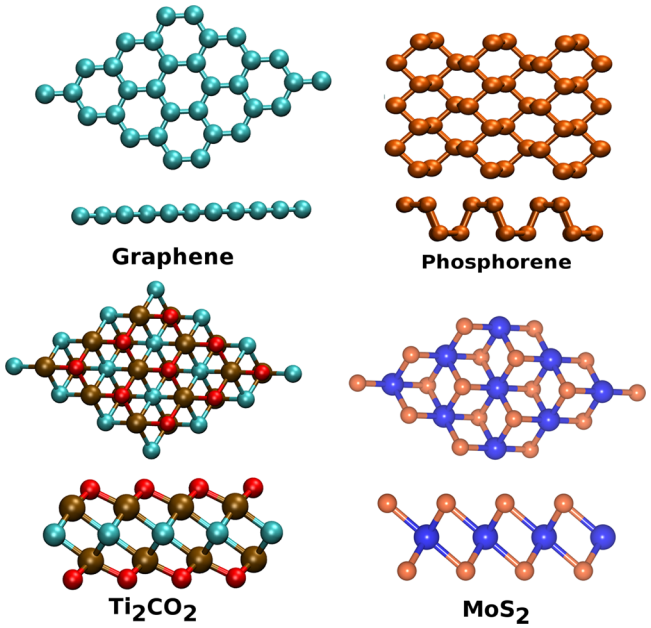

Figure 2. Crystal structure of some of the representative 2D materials.

characteristics of the 2D materials, which is vital for high speed transistors. Good ohmic contact and suitable band gap (≈1 eV) are other essential requirements for the high-performance transistor. Due to the high carrier mobility (2×10^5 cm^2 V^{-1} s^{-1}),[8] graphene was widely investigated, but it is not appropriate for applications in logic gates owing to its zero band gap, which results in small current on/off ratio (<10) at ambient temperature. Generating a band gap in graphene was proposed to enhance the performance of devices based on graphene; however, opening a band gap through engineering up to a value of ≈400 meV resulted in a significant reduction (>200 cm^2 V^{-1} s^{-1}) in the mobility.[9] Similarly, p-type devices constructed from graphene nanoribbons show an opening in the band gap due to different edge (zigzag or armchair) structures that resulted in high on/off ratio (10^6), but at a cost of extremely low charge carrier mobility of 100−200 cm^2 V^{-1} s^{-1}, as compared to other members of the graphene family. Another limitation with these devices is that they show high subthreshold slope (SS) of 210 mV per decade (i.e., increase in gate voltage needed, so that the drain current is changed by one decade, where decade denotes a ten times increase in drain current), which is very high compared to the desired value of 60 mV per decade.[5]

Compared to graphene, TMDCs such as MoS_2 (1.8), $MoTe_2$ (1.1), WS_2 (2.1 eV), and WSe_2 (1.7) possess desirable band gaps. Due to the suitable band gap, high on/off ratio, and low cost, MoS_2 has drawn significant attention as a promising material for logic devices such as a metal-oxide-semiconductor field-effect transistor (MOSFET). However, experimental results showed low carrier mobility (1 cm^2 V^{-1} s^{-1}) of MoS_2-based devices without high-K dielectric gate material. In contrast, the mobility can reach to a value of 150 cm^2 V^{-1} s^{-1} with HfO_2 used as a top gate layer at 300 K. On the other hand, theoretical calculations performed using density functional theory reported the mobility of 400 cm^2 V^{-1} s^{-1} for MoS_2 at room temperature.[5,9] In addition, layered black phosphorus[11] (another type of 2D material) is found to have a high mobility of 2.6×10^4 cm^2 V^{-1} s^{-1} theoretically, and experimentally, a mobility of 10^3 has been achieved, which shows its promising potential in electronic devices. Several other 2D materials have been investigated for logic devices, however with mobility less than the desired value. This review presents an overview of the methodologies adopted for mobility calculation in the theoretical research of 2D materials. It also shed light on the current challenges of theoretical methods and future prospects of the 2D materials in device applications.

METHODS

The carrier mobility of a charged particle characterizes how quickly it can move in a material when driven by an external electric field. The mobility strongly depends on the scattering phenomena within the material. Scattering caused by lattice vibrations determines intrinsic mobility and constitutes the upper limit for free-standing defectless 2D materials. Besides phonons, the other processes that contribute to the phenomenon of scattering are defects, which makes it challenging to measure intrinsic mobility experimentally; as such, it is usually calculated theoretically.[12] Several methods exist in the literature to calculate the electron/hole mobility such as the deformation potential theory (DPT)[7] and Boltzmann transport equation (BTE) using the electron−phonon coupling (EPC) matrix calculation method by which scattering rates and relaxation time are calculated from first principles.[12] The Boltzmann transport equation[13] (BTE) for electron distribution $f(\epsilon_{\mathbf{kn}}) = f_{\mathbf{kn}}$ reads

$$\frac{\partial f_{\mathbf{kn}}}{\partial t} + \mathbf{v}_{\mathbf{kn}} \cdot \nabla_{\mathbf{r}} f_{\mathbf{kn}} + \frac{\mathbf{F}}{\hbar} \cdot \nabla_{\mathbf{k}} f_{\mathbf{kn}} = \left(\frac{\partial f_{\mathbf{kn}}}{\partial t}\right)_{\mathbf{coll}} \quad (1)$$

where the labels $\mathbf{n}$ and $\mathbf{k}$ denote the band index and k point, respectively. The velocity is defined as $\mathbf{v} = 1/\hbar \nabla_{\mathbf{k}} \epsilon_{\mathbf{kn}}$, and $\mathbf{F} = q(\mathbf{E} + \mathbf{v} \times \mathbf{B})$ is the external force. The right-hand side of the above equation includes different scattering and dissipation sources that drive the system to equilibrium. For a homogeneous system in a static electric field and zero magnetic field, the BTE simplifies to

$$\frac{q\mathbf{E}}{\hbar} \cdot \nabla_{\mathbf{k}} f_{\mathbf{kn}} = \left(\frac{\partial f_{\mathbf{kn}}}{\partial t}\right)_{\mathrm{coll}} \quad (2)$$

Assuming collisions independent of the driving force, the collision integrals can be expressed using transition rates ($\mathbf{P}_{\mathbf{kk}'}^{\mathbf{nn}'}$):

https://dx.doi.org/10.1021/acsomega.0c01676
ACS Omega 2020, 5, 14203−14211

$$\frac{\partial f_{\mathbf{kn}}}{\partial t} = -\sum_{\mathbf{k'n'}} [f_{\mathbf{kn}}(1 - f_{\mathbf{k'n'}})\mathbf{P}^{\mathbf{nn'}}_{\mathbf{kk'}} - \mathbf{f}_{\mathbf{k'n'}}(\mathbf{1} - \mathbf{f}_{\mathbf{kn}}\mathbf{P}^{\mathbf{n'n}}_{\mathbf{k'k}})] \tag{3}$$

The transition rate from state $|\mathbf{kn}\rangle$ to $|\mathbf{k'n'}\rangle$ caused by phonon scattering is obtained from the golden rule of Fermi:[13]

$$\mathbf{P}^{\mathbf{nn'}}_{\mathbf{kk'}} = \frac{2\pi}{\hbar}\sum_{q,\lambda}|g^{\lambda\mathbf{nn'}}_{\mathbf{k}q}|^2[\mathbf{n}^{\lambda}_{q}\delta(\epsilon_{\mathbf{k'n'}} - \epsilon_{\mathbf{kn}} - \hbar\omega_{q\lambda})\delta_{\mathbf{k'},\mathbf{k}+q} + (\mathbf{n}^{\lambda}_{-q} + 1)\delta(\epsilon_{\mathbf{k'n'}} - \epsilon_{\mathbf{kn}} + \hbar\omega_{-q\lambda})\delta_{\mathbf{k'},\mathbf{k}+q}] \tag{4}$$

In eq 4, the first and last terms describe the absorption and emission of a phonon. The spontaneous emission is incorporated in the last term, which remains at zero temperature. The sum is performed over phonon momentum (q) with branch index (λ). $g^{\lambda\mathbf{nn'}}_{\mathbf{k}q}$ represents the electron−phonon coupling (EPC) matrix and is calculated employing the density functional perturbation theory. The EPC matrix is defined between Bloch states $|\mathbf{kn}\rangle$ and $|\mathbf{k'n'}\rangle$ and is given by $\langle\mathbf{n'k'}|\delta\hat{H}_{q\lambda}|\mathbf{nk}\rangle$, where $\delta\hat{H}$ is the perturbed Hamiltonian. In eq 4, $\mathbf{n}^{\lambda}_{q}$ is the equilibrium Bose−Einstein distribution ($\mathbf{n}^{\lambda}_{q} = \mathbf{n}^{0,\lambda}_{q}$), in which case $\mathbf{n}^{\lambda}_{q} = \mathbf{n}^{\lambda}_{-q}$, because $\omega^{\lambda}_{q} = \omega^{\lambda}_{-q}$. The transition rates $\mathbf{P}^{\lambda\mathbf{nn'}}_{\mathbf{k'k}}$ and $\mathbf{P}^{\lambda\mathbf{n'n}}_{\mathbf{kk'}}$ are connected through the detailed balance equation.

$$f^{0}_{\mathbf{kn}}(1 - f^{0}_{\mathbf{k'n'}})\mathbf{P}^{\mathbf{nn'}}_{\mathbf{kk'}} - f^{0}_{\mathbf{k'n'}}(1 - f^{0}_{\mathbf{kn}})\mathbf{P}^{\mathbf{n'n}}_{\mathbf{k'k}} = 0 \tag{5}$$

where f^0 is the equilibrium Fermi−Dirac distribution. Linearizing eq 2 by the equilibrium distribution in the electric field, we have

$$\frac{q\mathbf{E}}{\hbar}\nabla_{\mathbf{k}}f_{\mathbf{kn}} \approx \frac{q\mathbf{E}}{\hbar}\nabla_{\mathbf{k}}f^{0}_{\mathbf{kn}} = q\mathbf{E}\mathbf{v}_{\mathbf{kn}}\frac{\partial f^{0}_{\mathbf{kn}}}{\partial\epsilon_{\mathbf{kn}}} \tag{6}$$

The right-hand side of eq 2 is linearized by considering the linear distribution function in the electric field. Defining a generalized transport relaxation time[13] $\tau_{\mathbf{kn}}$, we have

$$f_{\mathbf{kn}} = f^{0}_{\mathbf{kn}} + q\mathbf{E}\mathbf{v}_{\mathbf{kn}}\tau_{\mathbf{kn}}\left(-\frac{\partial f^{0}_{\mathbf{kn}}}{\partial\epsilon_{\mathbf{kn}}}\right) \tag{7}$$

Making use of eqs 3−7, eq 2 reads

$$1 = \sum_{\mathbf{k'n'}}\mathbf{P}^{\mathbf{nn'}}_{\mathbf{kk'}}\frac{1 - f^{0}_{\mathbf{k'n'}}}{1 - f^{0}_{\mathbf{kn}}} \times \left[\tau_{\mathbf{kn}} - \tau_{\mathbf{k'n'}}\frac{n_{\mathbf{k'n'}}}{n_{\mathbf{kn}}}\frac{f^{0}_{\mathbf{kn}}(1 - f^{0}_{\mathbf{kn}})}{f^{0}_{\mathbf{k'n'}}(1 - f^{0}_{\mathbf{k'n'}})}\right] \tag{8}$$

Here, $\mathbf{n}_{\mathbf{kn}} = \hat{E}\hat{V}_{\mathbf{kn}}$, and eq 8 is still a full integral equation; however, several approximations exist in the literature to reduce the problem to a $\mathbf{k}'$ space integration, which are known as relaxation time approximations. For example, the term in brackets in eq 8 is replaced by $\tau_{\mathbf{kn}}$ times the normalized factor $\left[1 - \frac{\mathbf{kk'}}{\mathbf{kk'}}\right]$ and rarely by $\left[1 - \frac{\mathbf{v}_{\mathbf{kn}}\mathbf{v}_{\mathbf{kn}}}{|\mathbf{v}_{\mathbf{k'n'}}||\mathbf{v}_{\mathbf{kn}}|}\right]$. The normalized condition is related by the assumption that $\tau_{\mathbf{k'n'}} \approx \tau_{\mathbf{kn}}$, in which case the last Fermi factor is equal to unity. The relaxation time of the linearized BTE[13] including the inelastic scattering processes is defined as

$$\frac{1}{\tau_{\mathbf{kn}}} = \sum_{\mathbf{k'n'}}\frac{1 - f^{0}_{\mathbf{k'n'}}}{1 - f^{0}_{\mathbf{kn}}}\left[\frac{\mathbf{v}_{\mathbf{k'n'}}\mathbf{v}_{\mathbf{kn}}}{|\mathbf{v}_{\mathbf{k'n'}}||\mathbf{v}_{\mathbf{kn}}|}\right]\mathbf{P}^{\mathbf{nn'}}_{\mathbf{kk'}} \tag{9}$$

The mobility[12] μ can then be obtained using the equation

$$\mu = \frac{e\tau}{m^*} \tag{10}$$

where $|e|$ is the basic unit of charge; m^* denotes the effective mass of carriers; and τ is defined in eq 9.

Among these methods, the DPT due to its simplicity and being computationally less expensive has been extensively used to calculate the intrinsic mobility. In DPT, the carrier mobility is calculated by using the equation[7,14]

$$\mu_j = \frac{e\hbar^3 C_j}{k_B T m^*_j m_d(E^2_j)} \text{ where } j = x, y \tag{11}$$

where m^*_j is the carrier effective mass in direction of motion and $m_d = \sqrt{m^*_x m^*_y}$ represents the average of effective masses along x- and y-direction. The term E_i designates the deformation potential constant of holes and electrons in the valence band maximum and conduction band minimum, respectively, along the transport direction. It is defined as $E_j = \Delta V_j/\varepsilon$, where ΔV_j represents the change in energy of the j^{th} band under cell deformation (elongation and compression), and ε denotes the applied strain, which is given by $\varepsilon = \Delta a/a_0$; here a_0 and Δa are the optimized lattice constant and the deformation of a_0 along the transport direction, respectively. The elastic constants C_j along a given direction are obtained by parabolic fitting of the equation $(E - E_0)/A_0 = C_j\varepsilon^2/2$, where E is the calculated energy of the system under strain; E_0 and A_0 represent the energy and area of the equilibrium system; and T = 300 K. Equation 11 takes into account the effect of deformation potential, effective mass, and elastic constants along the transport direction only. However, most of the materials are anisotropic, and as such it is critical to incorporate the effect of these parameters along the transverse direction also. A modified form of eq 11 to incorporate the anisotropic[15] effect of 2D materials is given by

$$\mu_x = \frac{e\hbar^3\left(\frac{5C_x + 3C_y}{8}\right)}{k_B T m^{3/2}_x m^{1/2}_y\left(\frac{9E^2_x + 7E_xE_y + 4E^2_y}{20}\right)} \tag{12}$$

From eq 12, it can be easily noted that the carrier mobility depends on the parameters such as effective mass, elastic constants, and deformation potential not only along a given direction but in transverse direction also. It is essential to mention that DPT includes scattering due to the longitudinal acoustic (LA) phonon modes only and it presumes the electron−phonon coupling (EPC)to be isotropic. However, to obtain intrinsic mobility that is more accurate and reliable, it is required to calculate the matrix elements of EPC for each scattering process,[12] which is computationally expensive. Therefore, most of the theoretical studies used to calculate the mobility of carrier in 2D materials are performed using DPT.

TRANSPORT PROPERTIES OF 2D MATERIALS

Graphene. Graphene is the extensively studied 2D material because of its rich physics such as large thermal conductivity, high carrier mobility, and chiral behavior of the carriers. However, the band structure of pristine graphene shows zero band gap, and the symmetry of the honeycomb lattice at the k-points of the Brillouin zone preserves the zero band gap of the monolayer sheet. An external electric field can be used to tune

https://dx.doi.org/10.1021/acsomega.0c01676
ACS Omega 2020, 5, 14203−14211

the band gap of 2D materials, and by the application of the transverse electric field the band gap of bilayer graphene attained a value of 250 meV. In addition to the electric field, strain can also be employed to tailor the band gap of layered materials. For instance, the band gap decreases linearly in a mono- and bilayered MoS_2 at a rate of 45 and 120 meV per percent of strain, respectively. Moreover, the application of magnetic field can also be used to modify the electronic structure of 2D materials.[9]

Engineering the band gap of graphene increases fabrication complexities and diminishes mobilities to a level of strained silicon films. Band gaps up to 400 meV have been created in patterned or exfoliated nanoribbon graphene by quantum mechanical confinement but always at a cost of substantial reduction in mobility (200 $cm^2\ V^{-1}\ s^{-1}$ for a 150 meV band gap). Band gaps have also been introduced in bilayer graphene by an external electric field applied perpendicular to the surface, but the maximum optical band gap reported is 250 meV, which requires an external voltage exceeding 100 V. These limitations make it challenging to build logic gates based on graphene with low standby power dissipation working at room temperature. To potentially replace CMOS-like digital logic devices based on silicon, a current on/off ratio (I_{on}/I_{off}) between 10^4 and 10^7 and a bandgap exceeding 400 meV are indispensable.[9]

The chemical doping is a natural way to increase the performance or tailor the properties of graphene or any other 2D material. Efficient n-type (p-type) doping can be realized within the graphene lattice through the incorporation of nitrogen (boron) atoms, respectively. Roche and co-workers[16] theoretically studied the charge transport physics in chemically doped (using boron/nitrogen as dopants) disordered graphene by using ab initio derived diffusion potentials and a transport approach based on quantum-mechanical calculations. The mobility of electrons and holes so obtained was found to be asymmetric on either side of the Dirac point. Depending on doping concentration, the carrier mobility in disordered graphene was found to be in the range of 7×10^2 to $4 \times 10^2\ cm^2\ V^{-1}\ s^{-1}$ for $n(E) = 10^{12}$ electrons/holes. Singh and co-workers[14] functionalized graphene by codoping with boron and nitrogen/phosphorus elements. Their results show that the mobility of functionalized graphene was smaller than the pristine graphene. The calculated mobility of borocarbophosphide (BCP) was found to be $2.99 \times 10^3\ cm^2\ V^{-1}\ s^{-1}$ for electrons and $1.61 \times 10^3\ cm^2\ V^{-1}\ s^{-1}$ for holes. On the other hand, the mobility of borocarbonitride BCN was found to be $0.16 \times 10^3\ cm^2\ V^{-1}\ s^{-1}$ and $0.176 \times 10^3\ cm^2\ V^{-1}\ s^{-1}$ for electrons and holes, respectively. These reports have shown that the band gap can be produced in graphene by chemical doping but at the cost of significant reduction in its carrier mobility as evident from Table 1.

Transition Metal Dichalocogenides (TMDCs). MOSFET is a chief component of any logic device in modern technology. Any material considered for the development of a logic device (or logic gate) has to fulfill some basic requirements such as high current on/off switching ratio in the range of 10^4–10^7 and large carrier mobility for fast operation. A significant band gap of few layer or monolayer MoS_2 makes it a promising material for logic gates to provide high switching speed with low power consumption in the off state.[9] Although there has been an increasing interest in its electronic properties and device applications, the charge carrier mobility in MoS_2 has not reached a value to even compete with

Table 1. Band Gap (eV) and Mobility (Unit: $10^3\ cm^2\ V^{-1}\ s^{-1}$) of Some Representative 2D Materials at 300 K[a]

material	E_{gap}	μ_x^e	μ_x^h	μ_y^e	μ_y^h	ref
MoS_2	1.8	0.072	0.060	0.200	0.152	18
WS_2	1.54	0.12	0.21	–	–	18
α-P	1.0	1.14	0.08	0.70	26	11
Sb	1.8	0.045	0.034	0.015	0.016	7
$TiCO_2$	0.91	0.611	0.254	74.1	22.5	21
Hf_2CO_2	1.79	0.126	2.270	2.192	1.598	21
Zr_2CO_2	1.76	0.083	1.096	2.299	1.695	21
BCN	1.97	0.176	0.088	0.023	0.164	14
B_2Se_2	4.94	615	11.1	623	11.4	23
BCP	0.55	1.59	1.61	2.29	0.84	14
BP	0.91	49.96	13.70	68.81	26.05	23
BAs	0.46	39.28	16.92	57.78	32.46	23

[a]e, h denote the electron and hole, respectively.

silicon ($1400\ cm^2\ V^{-1}\ s^{-1}$). The electron mobility of MoS_2 was calculated to be on the order of $410\ cm^2\ V^{-1}\ s^{-1}$ at room temperature, and the mobility was found to be even smaller than the theoretical limit in actual devices. In an early study, Novoselovet al. reported low carrier mobility of MoS_2 in the range of 0.5 and $3\ cm^2\ V^{-1}\ s^{-1}$, which is far less than what is required for logic applications. Subsequently, it was found that ultrathin nanosheets of MoS_2 produced by mechanical exfoliation show high field effect mobility in tens of $cm^2\ V^{-1}\ s^{-1}$ and large (10^5) on/off ratio. Interestingly, in a top-gated MoS_2-based FET, extraordinarily high on/off ratio (10^8), significant mobility of carriers that can be above $60\ cm^2\ V^{-1}\ s^{-1}$, and SS of 74 mV/decade were reported at room temperature.[5,9] It should be noted that SS produces both qualitative and quantitative analysis of I_{on}/I_{off} ratio, and a FET with low value of SS shows better switching behavior and larger I_{on}/I_{off} number. The ideal value of SS at room temperature is 60 mV per decade. FET fabricated using monolayer MoS_2 has shown high on/off ratio (10^8) and carrier mobility of about $150\ cm^2\ V^{-1}\ s^{-1}$ once hafnium dioxide (HfO_2) was used as a dielectric material for the gate layer.[5,17]

Other than MoS_2, WSe_2, which is a p-type material, which is also bestowed with properties such as direct band gap (1.65 eV), is desired for device applications. A p-type FET based on mechanically exfoliated monolayer WSe_2 has shown better mobility of $\sim 250\ cm^2\ V^{-1}\ s^{-1}$ for holes, suitable on/off current ratio of 10^6, and ideal SS slope of 60 mV/decade. On the other hand, a p-type FET constructed from a chemical vapor deposition grown monolayer WSe_2 exhibited $\sim 90\ cm^2\ V^{-1}\ s^{-1}$ hole mobility and 10^5 on/off current ratio. Similarly, it is shown that FETs built from $MoTe_2$ show ambipolar nature. Thus, by controlling methods, both p- and n-type materials can be produced. The mobility of $200\ cm^2\ V^{-1}\ s^{-1}$ at room temperature has been found in the $MoTe_2$-based FET from theoretical calculations;[5] however, experimental work reported that trilayered $MoTe_2$-based devices with Ti contacts show a carrier mobility of 7×10^{-2} (2×10^{-2}) for holes (electrons). In another work, a $MoTe_2$-based device with Au contacts was found to show enhanced mobility of $16.5\ cm^2\ V^{-1}\ s^{-1}$ and on/off current ratio of 10^7. Sarkar and co-workers[18] investigated the carrier mobility of TMDCs (MoX_2, where M = Mo, W; X = S, Se, and Te) and found that mobility is maximum for WS_2 with values of about $0.12 \times 10^3\ cm^2\ V^{-1}\ s^{-1}$ and $0.21 \times 10^3\ cm^2\ V^{-1}\ s^{-1}$ for the electron and hole, respectively, along the x-direction. For all other systems, they found that mobility is less

https://dx.doi.org/10.1021/acsomega.0c01676
ACS Omega 2020, 5, 14203−14211

than 100 $cm^2\ V^{-1}\ s^{-1}$. The authors also claimed that sulfides show superior mobility compared to the selenides and tellurides.

Considering the current FET applications of TMDC materials, the main focus among the material properties is on carrier mobility. It is critical to recognize that impurities present in material lead to a screening effect that, in turn, affects the charge carrier dielectric environment. The gate layer has large dielectric constant due to which the capacitive coupling increases between the top and back gates, thus inciting the mobility of carriers by 10 to 50 times. Also, the carrier mobility in a FET based on single or few-layer MoS_2 obtained at room temperature is about 10 $cm^2\ V^{-1}\ s^{-1}$ if the substrate (Si/SiO_2) used is without a high-k dielectric gate layer. Thus, a poor interface between MoS_2 and Si/SO_2 is one of the factors for low mobility in the FETs. The interface problem includes surface defects, distribution of local charges, and concentration of charged impurities. Besides, charges trapped in the substrate cause Coulomb scattering, which leads to lower mobility values. However, using high-k dielectric material such as alumina (Al_2O_3) or HfO_2 as the top gate layer, the mobility is increased to a value of 150 $cm^2\ V^{-1}\ s^{-1}$ in a monolayer MoS_2 device due to the screening effect.[5,9]

2D Phosphorus. Phosphorene[7] (α-P) is another representative member of 2D materials that has garnered immense research interest as it exhibits unusual properties and enormous potential in the electronic application field. Due to its finite bandgap of 1 eV, the α-P is a strong competitor of graphene from the application point of view. α-P is a 2D format of black phosphorus and has been successfully produced in 2014 through mechanical exfoliation techniques. At room temperature, it exhibits high on/off current ratio and ambipolar charge transport of $\sim 1 \times 10^4$. Wei and co-workers[11] have found the carrier mobility of mono- and few-layer α-phosphorene. They found that the mobility is reasonably high ($\sim 10^2-10^4\ cm^2\ V^{-1}\ s^{-1}$), anisotropic, and antisymmetric between holes and electrons. In particular, holes were found to be more mobile than electrons. Their predicted values of electron mobilities in monolayer α-P were $1.1-1.14 \times 10^3\ cm^2\ V^{-1}\ s^{-1}$ and 80 $cm^2\ V^{-1}\ s^{-1}$ along the x- and y-directions, respectively. Hole mobility of monolayer α-P was found to be $0.64-0.70 \times 10^3\ cm^2\ V^{-1}\ s^{-1}$ in the x-direction and $10-26 \times 10^3\ cm^2\ V^{-1}\ s^{-1}$ in the y-direction. The large hole mobility compared to electrons was ascribed to the difference in deformation potential of the carriers. Further, Zheng and co-worker[19] investigated the mobility of mono- and few-layer α-P systems, and their results have shown that the highest carrier mobility occurs in monolayer systems with values of $1.6 \times 10^3\ cm^2\ V^{-1}\ s^{-1}$ and $2.21 \times 10^4\ cm^2\ V^{-1}\ s^{-1}$ for electrons and holes, respectively. They also tailored the carrier mobility in α-P by applying strain and found that the hole mobility increases to a value of $2.62 \times 10^5\ cm^2\ V^{-1}\ s^{-1}$ under 10% strain, and the mobility is exceptionally high, namely, 10 times larger than that in the strain-free case. It was also seen that mobility increases with applied strain up to 10% and decreases beyond that value of strain.[19]

The rapid development in the FETs based on phosphorene started in 2014 and has been continuously growing since then (see ref 20 and references therein). Compared to the other 2D semiconductors, FETs based on phosphorene are considered to show improved performance due to their anisotropic charge transport. Das et al.[19] demonstrated the electron and hole transport in a FET based on few-layer phosphorene using 20 nm thick SiO_2 as the back gate dielectric and titanium as the drain/source contact electrode. The measured field effect mobility was ~38 and ~172 $cm^2\ V^{-1}\ s^{-1}$ for the electrons and holes, respectively. The on/off current ratios obtained were $\sim 4.4 \times 10^3$ for electrons and $\sim 2.7 \times 10^4$ for holes. In another study, a few-layer phosphorene-based FET also using the SiO_2 as a gate insulator was demonstrated to exhibit p-type behavior.[5] They found that with an increase in sample thickness the drain current modulation decreases monotonically, while it was seen that mobility attained a maximum value at 10 nm thickness and then decreased slowly. The FET showed ambipolar nature with field effect mobility reaching a value of 984 $cm^2\ V^{-1}\ s^{-1}$ and drain current modulation of 10^5 at room temperature. However, the critical part about these FETs is the degradation of phosphorene material with thinner films at the interface being more prone to charge impurities.

The performance of FETs can be improved by using high-k dielectrics as a gate insulator. HfO_2 is one of the high-k dielectric materials having a dielectric constant of 25 that is larger than that of SiO_2 by six times. Using the CMOS process at low temperature, FETs based on few-layer phosphorene displayed high performance when integrated with high-k dielectrics such as HfO_2. The fabricated device exhibited better SS of ~69 mV per decade, which is a near-ideal value of SS, low gate leakage current of 0.1 nA, and hole mobility more than 400 $cm^2\ V^{-1}\ s^{-1}$ at room temperature. Doping few-layer phosphorene with metal elements is another pathway to gain high performance and more stable phosphorene-based FETs. Theoretical calculations showed that Cu adatoms act as electron donors and produce an n-type doping effect in few-layer phosphorene without disturbing the structural integrity. It has been observed that doping few-layer phosphorene with Cu changes the threshold voltage, converts the phosphorene channel from p-type to n-type layer, and increases electron mobility from 1780 to 2140 $cm^2\ V^{-1}\ s^{-1}$ but at low temperature (7 K). Further, it was found that Te-doped phosphorene-based FETs show good electron mobility of 1850 $cm^2\ V^{-1}\ s^{-1}$ at room temperature. Also, nuclear magnetic resonance and atomic force microscopy showed that degradation of phosphorene at ambient conditions was markedly reduced by Te doping.[20]

Several studies have investigated A_2O_3 as a gate dielectric in phosphorene FETs as the degradation of phosphorene is a pressing concern regarding its practical applications. However, it was seen that fixed negative charge originates from the A_2O_3 layer that produces band bending at the interface of A_2O_3 and phosphorene. The degradation limits performance of phosphorene-based FETs prepared under ambient conditions. Therefore, it is essential to prepare devises in an environment with low humidity and oxygen content. Encapsulation using another material such as boron nitride will be helpful for devices to be operated at ambient conditions. Once these difficulties are overcome, phosphorene-based FETs could be promising for next-generation electronic devices.[11,19]

MXenes. Another member of the 2D family is materials derived from transition metal carbides, nitrides, or carbonitrides and is referred to as MXenes (pronounced as maxenes). The combination of their exceptional physical and chemical properties makes MXenes a rapidly growing family of layered materials. Research on 2D MXenes commenced in 2011, with the synthesis and separation of monolayers of titanium carbide (Ti_3C_2) for the first time. The work initiated worldwide theoretical and experimental studies on 2D carbides and

https://dx.doi.org/10.1021/acsomega.0c01676
ACS Omega 2020, 5, 14203−14211

nitrides and paved the way to the discovery of many more MXenes. The general formula of MXenes is $M_{m+1}X_mT_x$ (m = 1, 2, or 3) where M can be an early transition element; X is carbon and/or nitrogen; and T_x denotes surface termination group such as OH, F, and/or O atoms, with MXenes terminated by O and OH groups being the most stable ones.[6]

Most of the MXenes produced so far such as Ti_2C, V_2C, Nb_2C, Ti_3C_2, Ta_4C_2, Ti_3CN, etc. are metallic with a few being semiconductors, e.g., Ti_2CO_2. The mobility of Ti_2CO_2 was studied by Zhen and co-workers along the x- and y-direction using the DPT approach.[21] The calculated mobility of Ti_2CO_2 was 6.11 × 10^2 cm^2 V^{-1} s^{-1} along the x-direction and 2.54 × 10^2 cm^2 V^{-1} s^{-1} along the y-direction for electrons. The hole mobility was found to be 2 orders of magnitude more than electrons, as shown in Table 1. The carrier mobility is anisotropic, which is nearly three times larger along the x- than in the y-direction. As mentioned, the hole mobility is substantially higher along the x- and y-directions, a property that is useful for the separation of electrons and holes in photocatalysis. Further, to investigate the effect of layer numbers on the carrier mobility, a bilayer system Ti_2CO_2 was considered. It was reported that the carrier mobility remains anisotropic, and the differences between electron and hole mobility still exist. The hole mobility in bilayer Ti_2CO_2 was found to be 32.1 times higher along the x-direction and 11.6 times larger in the y-direction than electrons, as shown in Table 1. Additionally, they also investigated the mobility in a series of armchair nanoribbons with different widths. It was reported that the band gap in armchair nanoribbons of Ti_2CO_2 oscillates, and the amplitude of the oscillations decreased as the width increased. The reports showed that the mobility presents an increasing trend and reached a value of 6 × 10^3 cm^2 V^{-1} s^{-1}, while the electron mobility was seen to oscillate in a range of 5−55 cm^2 V^{-1} s^{-1}.[21]

Moreover, Zhimei and co-workers[21] studied the carrier mobility of $HfCO_2$ and $ZrCO_2$, and like Ti_3CO_2, the carrier mobility was found to exhibit anisotropic behavior. The ten times higher mobility of electrons in the y-direction than in the x-direction was attributed to the smaller effective mass of electrons along the y-axis. On the other hand, the hole mobility exhibited about 50% larger value in the x-direction than that of the y-direction. That is, the movement of charge carriers in 2D Zr_2CO_2 and Hf_2CO_2 is anisotropic. This anisotropy is such that electrons readily move along the y-direction, while holes tend to migrate easily in the x-direction. The calculated carrier mobilities 0.126 × 10^3 (0.0826 × 10^3) cm^2 V^{-1} s^{-1} and 2.27 × 10^3 (1.096 × 10^3) cm^2 V^{-1} s^{-1} for Hf_2CO_2 ($ZrCO_2$) along the x- and y-direction. The hole mobilities were found to be 22.19 × 10^3 (2.299 × 10^3) cm^2 V^{-1} s^{-1} and 1.598 (1.695) cm^2 V^{-1} s^{-1} along the x- and y-direction, respectively, for Hf_2CO_2 ($ZrCO_2$). It is clear from these results that carrier mobility is anisotropic with holes being more mobile than electrons (Figure 3).

Other 2D Materials. Recently, researchers also investigated other group V monolayered arsenene (As) and antimone (Sb).[22] Multilayered nanoribbons of As and Sb have been experimentally synthesized on InAs/InSb substrates. The mono- and few-layer Sb were produced using epitaxy growth and mechanical and liquid-phase exfoliation techniques. From the study of transport properties of monolayer Sb and As using DPT, it was found that the mobility of electrons is 635 cm^2 V^{-1} s^{-1} for As and 630 cm^2 V^{-1} s^{-1} for Sb, while the hole mobility obtained was 1700 cm^2 V^{-1} s^{-1} and 1737 cm^2 V^{-1} s^{-1} for Sb and As, respectively. Singh and co-workers[22] investigated the mobility of mono- and few-layer Sb also using DPT and found that in contrast to α-P mobility is dominated by electrons in Sb systems. They also reported that with the increase in the number of layers the mobility of carriers also increases. The calculated mobility of monolayer Sb was less than 100 cm^2 V^{-1} s^{-1}. Thus, we see that a significant difference in the calculated mobility is observed for Sb in the calculations. It was inferred that such differences arise from the different flavors (pseudopotentials, exchange-correlation functional, spin−orbit effects) used in DFT calculations. On the other hand, Liu and co-workers[23] used BTE and obtained an exceptionally high intrinsic mobility of ∼300 cm^2 V^{-1} s^{-1} for holes in monolayer Sb at room temperature, which is much higher than that predicted using DPT. The authors attributed the low mobility to spin−orbit coupling which earlier studies have not incorporated in their calculations.

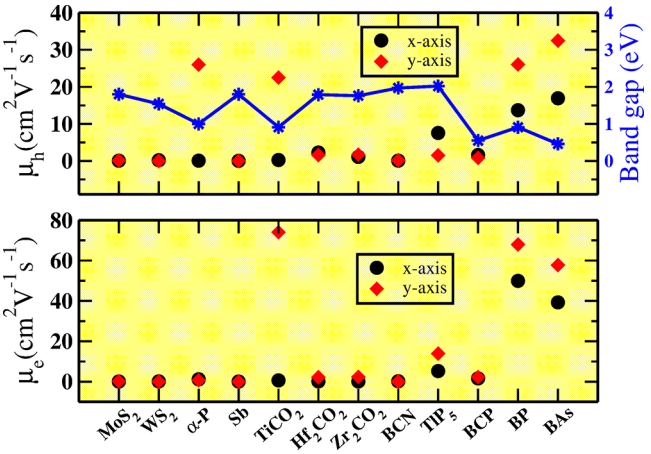

Figure 3. Graphical visualization of carrier mobility (× 10^3) and band gap values of some representative 2D materials.

Lu and co-workers[23] found that the carrier mobility of monolayer As is considerably low (21/66 cm^2 V^{-1} s^{-1} for electron/hole) and moderate in monolayer Sb (150/510 cm^2 V^{-1} s^{-1} for electron/hole). The authors investigated the electron−phonon interaction for three acoustic modes and found that the out-of-plane longitudinal phonon mode is the dominant factor for electron−phonon scattering and limits the mobility to such a low value. From these results, it is seen that As and Sb are stable at ambient conditions; however, their mobility values were significantly lower than that of α-P as depicted in Table 1.

Several other 2D materials such as boron pnictides (BX: X = P, As, and Sb) were investigated by Du and co-workers,[24] and they reported ultrahigh carrier mobility for these semiconductors. The mobility of BX is comparable to graphene and has an advantage over graphene as it exhibits direct band gaps of 1.36, 1.14, and 0.49 eV for BP, BAs, and BSb, respectively. In particular, the mobility of electrons in monolayered BSb was found to be of the order of graphene. The calculated mobilities for BX are reported in Table 1. Monolayer boron dichalcogenide (B2 × 2, X = S, Se, and Te) with hexagonal symmetry was found to be highly stable with band gaps that range from 2.14 to 4.01 eV. They also studied the mobility of these materials and found that Be_2Se_2 showed the highest mobility of 6.23 × 10^5 cm^2 V^{-1} s^{-1} for electrons and 1.13 × 10^4 cm^2 V^{-1} s^{-1} for holes and is anisotropic. In another study, Du and co-workers[25] investigated a novel kind

https://dx.doi.org/10.1021/acsomega.0c01676
ACS Omega 2020, 5, 14203−14211

of highly stable 2D AuSe with superior carrier mobility and high in-plane anisotropy. They also claimed that 2D AuSe could be peeled off from its layered bulk counterpart readily as it has low cleavage energy. Most importantly, it was seen that linear (Au^{II}) and square-planar (Au^{IV}) channels coexist in 2D AuSe, which leads to a notable in-plane anisotropic distribution of carriers and transport properties. It was found that the mobility of electrons dominates along the *x*-direction and can be as large as 3.98×10^4 cm^2 V^{-1} s^{-1}. In contrast, the mobility of holes predominate along the *y*-direction is over 8×10^3 cm^2 V^{-1} s^{-1}, which is about 40 times higher than the mobility along the *x*-direction. Although the above studies claim remarkably high carrier mobility for the 2D materials, nevertheless it is important to verify such claims through experiment.[23]

FUTURE PROSPECTS AND CONCLUDING REMARKS

Interest in low-dimensional materials is increasing day-by-day across the scientific community due to their exciting properties, which enable them to qualify as an important class of materials for the next electronic generations. However, their applications are strongly restricted either due to low intrinsic carrier mobility or a decrease in the mobility due to the substrate effect when used in a device such as FET. Although several electronic applications of graphene have been explored because of its exceptionally high carrier mobility, its zero band gap, which results in low on/off current ratio, has severely limited its practical applications for electronic devices. Different methods have been employed to improve the mobility of 2D materials such as doping, strain engineering, creating heterostructures, or multilayered systems, but none of the material has reached mobility values comparable to silicon in devices. For instance, the carrier mobility of mono- or few-layered MoS_2 measured experimentally is much smaller than that predicted theoretically (410 cm^2 V^{-1} s^{-1}).[17] In a semiconductor channel, scattering of lattice phonons induced by interfacial phonons, charged impurities, and high-*k* dielectric environment is one of the causes for low carrier mobility.[5] The scattering of charge carriers can occur by lattice phonons via deformation potential. Phonon scattering depends on temperature and thus increases as the temperature rises. Based on first-principles calculations of scattering of acoustic/polar phonons and screening of monolayer MoS_2, it is reported that mobility[17] of 410 cm^2 V^{-1} s^{-1} can be achieved; however, these calculations have not deduced the effect of free carrier screening and dielectric mismatch.

The phonon scattering becomes dominant due to the presence of high-dielectric material, which causes a reduction of room-temperature mobility. In TMDC compounds like MoS_2, the dipole moment produced between the cation and anion was due to the polar nature of the chemical bond. The electric field created by the perturbation of dipole moment of polar phonons interacts with charge carriers, which results in low mobility of the carrier. This process is known as polar optical phonon scattering or Frohlich interaction. The charge carriers can excite phonons if the polar vibrational mode is supported by the dielectric layer in FETs. Such phonons own remote interface or surface optical phonons. Scattering due to surface optical phonons at room temperature is dominated by a high dielectric environment compared to the low-*k* dielectric layer. Moreover, other than Coulomb and phonon scattering, structural defects also play a critical role in the reduction of carrier mobility. For instance, ion vacancy may act as a source of strong scattering in a low-quality sample. It has been reported that a high percentage of sulfur vacancy (0.4%) in mechanically exfoliated or CVD-grown MoS_2 affects the carrier mobility.[5]

Further, we shed light on the theoretical aspects of intrinsic mobility of carriers in some of the most widely studied 2D materials. We found that DPT has been broadly used to calculate the intrinsic mobility owing to its simplicity. However, the DPT considers only the longitudinal acoustic (LA) phonon scattering through the deformation of the unit cell. Moreover, it presumes isotropic coupling between electrons and phonons independent of the direction of electron/phonon momentum. These simplifications produce inaccurate results when there is a significant contribution to the scattering from optical phonons. Few modifications were made to the conventional DPT to take into account the scattering effects caused by optical phonons and piezoelectricity; nevertheless, these improvements are still approximate. The overestimation of the mobility from experimental results is due to improper treatment of the electron−phonon interaction and ignoring various scattering processes in theoretical methods. Even considering the calculations performed using appropriate physical models, discrepancies still exist among the theoretically calculated mobility in 2D materials. This can be attributed to the different flavors (pseudopotentials, exchange-correlation functional, and spin−orbit coupling) of DFT used in the calculations. Nevertheless, the accurate calculation of intrinsic carrier mobility is critical before any practical application of a 2D material; as such, it is important to overcome the limitations of DPT.

An alternate approach is to calculate the EPC matrix elements for each scattering process, but the method is computationally very expensive as it requires the calculation of Hessian. Even though remarkable and outstanding progress in the research of 2D materials continues to evolve, there is still much to learn about controllable engineering of 2D materials to improve the carrier mobility, which underpins future technologies. Thus, it is important to address two significant gaps to enable the design of low-dimensional materials at rapid progress with desired electronic properties and mobility. First, to cope with the functionalities of 2D materials, there is an urgent need for computational techniques that are reliable and accurate enough. Second, all the information generated in experimental measurements must be fully availed to provide input to computational methods; this ultimately will be useful in predicting novel materials and help to understand their behavior.

AUTHOR INFORMATION

Corresponding Author

Jayant Kumar Singh − *Department of Chemical Engineering, IIT Kanpur, Kanpur 208016, India; Prescience Insilico Private Limited, Bangalore 560049, India;* orcid.org/0000-0001-8056-2115; Email: jayantks@iitk.ac.in

Authors

Showkat Hassan Mir − *Department of Chemistry, IIT Kanpur, Kanpur 208016, India;* orcid.org/0000-0002-9291-4680

Vivek Kumar Yadav − *Department of Chemical Engineering, IIT Kanpur, Kanpur 208016, India;* orcid.org/0000-0002-9142-4567

Complete contact information is available at: https://pubs.acs.org/10.1021/acsomega.0c01676

https://dx.doi.org/10.1021/acsomega.0c01676
ACS Omega 2020, 5, 14203−14211

Notes

The authors declare no competing financial interest.

Biographies

Dr. Showkat Hassan Mir received his M.Sc. from the University of Kashmir in 2011 and Ph.D. from Central University of Gujarat, India. His current research interests are electronic properties of 2D materials and their applications for electronic and environmental sustainability.

Dr. Vivek Kumar Yadav received his Ph.D. from the Department of Chemistry, Indian Institute of Technology Kanpur under the supervision of Prof. Amalendu Chandra in 2014. He worked as a PostDoctoral fellow with Prof. Michael L. Klein at Temple University, Philadelphia, USA, before joining Prof. Singh's lab at IIT Kanpur. His area of interest is computational study of 2D materials for energy and environment, ab initio molecular dynamics of liquids at ambient, and supercritical conditions.

Prof. Jayant Kumar Singh received his B.Tech from IIT Kanpur in chemical engineering in 1997, M.Sc. in computer science and engineering in 2002, and Ph.D. in chemical engineering in the area of molecular simulation from SUNY Buffalo, USA, in 2004. He currently holds Mr. and Mrs. Gian Singh Bindra Chair Professor at the Department of Chemical Engineering of IIT Kanpur. Prof. Singh's current research interest is in material modeling, controlling interfacial behavior, nucleation phenomena, and development of molecular simulation tools.

■ ACKNOWLEDGMENTS

S.H.M. gratefully acknowledges the Institute Postdoctoral fellowship (IPDF) from the Department of Chemistry at IIT Kanpur. V.K.Y. acknowledges the funding from the Department of Science and Technology (MHRD F. NO. 5-6/2013 TS-VII). The HPC centre IIT Kanpur is acknowledged for providing the computational facility.

■ REFERENCES

(1) Geim, A. K.; Novoselov, K. S. The rise of graphene. *Nat. Mater.* **2007**, *6*, 183−191.
(2) Zeng, M.; Xiao, Y.; Liu, J.; Yang, K.; Fu, L. Exploring two-dimensional materials toward the next-generation circuits: from monomer design to assembly control. *Chem. Rev.* **2018**, *118*, 6236−6296.
(3) Zhang, H.; Chhowalla, M.; Liu, Z. 2D nanomaterials: graphene and transition metal dichalcogenides. *Chem. Soc. Rev.* **2018**, *47*, 3015−3017.
(4) Zhao, Q.; Guo, Y.; Zhou, Y.; Yao, Z.; Ren, Z.; Bai, J.; Xu, X. Band alignments and heterostructures of monolayer transition metal trichalcogenides MX3 (M= Zr, Hf; X= S, Se) and dichalcogenides MX2 (M= Tc, Re; X= S, Se) for solar applications. *Nanoscale* **2018**, *10* (7), 3547−3555.
(5) Ahmed, S.; Yi, J. Two-dimensional transition metal dichalcogenides and their charge carrier mobilities in field-effect transistors. *Nano-Micro Lett.* **2017**, *9* (4), 50.
(6) Gogotsi, Y.; Anasori, B. The Rise of MXenes. *ACS Nano* **2019**, *13* (8), 8491−8494.
(7) Mir, S. H. Exploring the electronic, charge transport and lattice dynamic properties of two-dimensional phosphorene. *Phys. B* **2019**, *572*, 88−93.
(8) Bolotin, K. I.; Sikes, K. J.; Jiang, Z.; Klima, M.; Fudenberg, G.; Hone, J.; Kim, P.; Stormer, H. L. Ultrahigh electron mobility in suspended graphene. *Solid State Commun.* **2008**, *146* (9−10), 351−355.
(9) Radisavljevic, B.; Radenovic, A.; Brivio, J.; Giacometti, V.; Kis, A. Single-layer MoS_2 transistors. *Nat. Nanotechnol.* **2011**, *6*, 147−150.
(10) Shavanova, K.; Bakakina, Y.; Burkova, I.; Shtepliuk, I.; Viter, R.; Ubelis, A.; Beni, V.; Starodub, N.; Yakimova, R.; Khranovskyy, V. Application of 2D non-graphene materials and 2D oxide nanostructures for biosensing technology. *Sensors* **2016**, *16* (2), 223.
(11) Qiao, J.; Kong, X.; Hu, Z. X.; Yang, F.; Ji, W. High-mobility transport anisotropy and linear dichroism in few-layer black phosphorus. *Nat. Commun.* **2014**, *5* (1), 1−7.
(12) Cheng, L.; Liu, Y. What Limits the Intrinsic Mobility of Electrons and Holes in Two Dimensional Metal Dichalcogenide. *J. Am. Chem. Soc.* **2018**, *140*, 17895−17900.
(13) (a) Gunst, T.; Markussen, T.; Stokbro, K.; Brandbyge, M. First-principles method for electron-phonon coupling and electron mobility: Applications to two-dimensional materials. *Phys. Rev. B: Condens. Matter Mater. Phys.* **2016**, *93* (3), 035414. (b) Sohier, T.; Calandra, M.; Park, C. H.; Bonini, N.; Marzari, N.; Mauri, F. Phonon-limited resistivity of graphene by first-principles calculations: Electron-phonon interactions, strain-induced gauge field, and Boltzmann equation. *Phys. Rev. B: Condens. Matter Mater. Phys.* **2014**, *90* (12), 125414.
(14) Yadav, V. K.; Mir, S. H.; Singh, J. K. A computational study of structural, electronic and carrier mobility of boron and phosphorus/nitrogen co-doped graphene. *Phys. B* **2019**, *571*, 291−295.
(15) Zhou, M.; Chen, X.; Li, M.; Du, A. Widely tunable and anisotropic charge carrier mobility in monolayer tin (II) selenide using biaxial strain: a first-principles study. *J. Mater. Chem. C* **2017**, *5*, 1247−1254.
(16) Lherbier, A.; Blase, X.; Niquet, Y. M.; Triozon, F.; Roche, S. Charge transport in chemically doped 2D graphene. *Phys. Rev. Lett.* **2008**, *101*, 036808−4.
(17) Yu, Z.; Ong, Z. Y.; Pan, Y.; Cui, Y.; Xin, R.; Shi, Y.; Wang, B.; Wu, Y.; Chen, T.; Zhang, Y. W.; Zhang, G. Realization of Room-Temperature Phonon-Limited Carrier Transport in Monolayer MoS2 by Dielectric and Carrier Screening. *Adv. Mater.* **2016**, *28* (3), 547−552.
(18) Rawat, A.; Jena, N.; De Sarkar, A. A comprehensive study on carrier mobility and artificial photosynthetic properties in group VI B transition metal dichalcogenide monolayers. *J. Mater. Chem. A* **2018**, *6*, 8693−8704.
(19) (a) Fang, R.; Cui, X.; Khan, M. A.; Stampfl, C.; Ringer, S. P.; Zheng, R. Strain-Engineered Ultrahigh Mobility in Phosphorene for Terahertz Transistors. *Adv. Electron. Mater.* **2019**, *5*, 1800797. (b) Das, S.; Demarteau, M.; Roelofs, A. Ambipolar phosphorene field effect transistor. *ACS Nano* **2014**, *8* (11), 11730−11738.
(20) (a) Liu, B.; Fathi, M.; Chen, L.; Abbas, A.; Ma, Y.; Zhou, C. Chemical vapor deposition growth of monolayer WSe2 with tunable device characteristics and growth mechanism study. *ACS Nano* **2015**, *9* (6), 6119−6127. (b) Wang, X.; Ouyang, Y.; Li, X.; Wang, H.; Guo, J.; Dai, H. Room-temperature all-semiconducting sub-10-nm graphene nanoribbon field-effect transistors. *Phys. Rev. Lett.* **2008**, *100* (20), 206803.
(21) (a) Zhang, X.; Zhao, X.; Wu, D.; Jing, Y.; Zhou, Z. High and anisotropic carrier mobility in experimentally possible Ti2CO2 (MXene) monolayers and nanoribbons. *Nanoscale* **2015**, *7*, 16020−16025. (b) Guo, Z.; Zhou, J.; Zhu, L.; Sun, Z. MXene: a promising photocatalyst for water splitting. *J. Mater. Chem. A* **2016**, *4*, 11446−11452.
(22) (a) Mir, S. H.; Yadav, V. K.; Singh, J. K. Unraveling the stacking effect and stability in nanocrystalline antimony through DFT. *J. Phys. Chem. Solids* **2020**, *136*, 109156. (b) Pizzi, G.; Gibertini, M.; Dib, E.; Marzari, N.; Iannaccone, G.; Fiori, G. Performance of arsenene and antimonene double-gate MOSFETs from first principles. *Nat. Commun.* **2016**, *7*, 12585.
(23) (a) Wang, Y.; Huang, P.; Ye, M.; Quhe, R.; Pan, Y.; Zhang, H.; Zhong, H.; Shi, J.; Lu, J. Many-body effect, carrier mobility, and device performance of hexagonal arsenene and antimonene. *Chem. Mater.* **2017**, *29*, 2191−2201. (b) Cheng, L.; Zhang, C.; Liu, Y. The Optimal Electronic Structure for High-Mobility 2D Semiconductors: Exceptionally High Hole Mobility in 2D Antimony. *J. Am. Chem. Soc.* **2019**, *141* (41), 16296−16302.
(24) Tang, C.; Ma, F.; Zhang, C.; Jiao, Y.; Matta, S. K.; Ostrikov, K.; Du, A. 2D boron dichalcogenides from the substitution of Mo with

https://dx.doi.org/10.1021/acsomega.0c01676
ACS Omega 2020, 5, 14203−14211

ionic B2 pair in MoX2 (X= S, Se and Te): high stability, large excitonic effect and high charge carrier mobility. *J. Mater. Chem. C* **2019**, *7* (6), 1651−1658.
(25) Tang, C.; Zhang, L.; Zhang, C.; MacLeod, J.; Ostrikov, K. K.; Du, A. Highly stable two-dimensional gold selenide with large in-plane anisotropy and ultrahigh carrier mobility. *Nanoscale Horizons* **2020**, *5*, 366−371.

https://dx.doi.org/10.1021/acsomega.0c01676
ACS Omega 2020, 5, 14203−14211